Opto-Electronic Advances

Article

July 2023, Vol. 6, No. 7

DOI: 10.29026/oea.2023.230007

Deep-red and near-infrared organic lasers based on centrosymmetric molecules with excited-state intramolecular double proton transfer activity

Chang-Cun Yan[1,2,3†], Zong-Lu Che[2†], Wan-Ying Yang[2], Xue-Dong Wang[2*] and Liang-Sheng Liao[1,2*]

Organic lasers that emit light in the deep-red and near-infrared (NIR) region are of essential importance in laser communication, night vision, bioimaging, and information-secured displays but are still challenging because of the lack of proper gain materials. Herein, a new molecular design strategy that operates by merging two excited-state intramolecular proton transfer-active molecules into one excited-state double proton transfer (ESDPT)-active molecule was demonstrated. Based on this new strategy, three new materials were designed and synthesized with two groups of intramolecular resonance-assisted hydrogen bonds, in which the ESDPT process was proven to proceed smoothly based on theoretical calculations and experimental results of steady-state and transient spectra. Benefiting from the effective six-level system constructed by the ESDPT process, all newly designed materials showed low threshold laser emissions at approximately 720 nm when doped in PS microspheres, which in turn proved the existence of the second proton transfer process. More importantly, our well-developed NIR organic lasers showed high laser stability, which can maintain high laser intensity after 12000 pulse lasing, which is essential in practical applications. This work provides a simple and effective method for the development of NIR organic gain materials and demonstrates the ESDPT mechanism for NIR lasing.

Keywords: excited-state intramolecular proton transfer; organic laser; near-infrared emission; molecular design

Yan CC, Che ZL, Yang WY, Wang XD, Liao LS. Deep-red and near-infrared organic lasers based on centrosymmetric molecules with excited-state intramolecular double proton transfer activity. *Opto-Electron Adv* **6**, 230007 (2023).

Introduction

Organic solid-state lasers (OSSLs) with light weight, tunable emission wavelengths, mechanical flexibility and simple fabrication processes have been intensively investigated in terms of material development, device design and mechanism study[1–5]. Notably, compared to visible OSSLs, near-infrared (NIR) organic lasers, which are potentially applied in laser communication, night

[1]Macao Institute of Materials Science and Engineering, Macau University of Science and Technology, Taipa, Macau SAR 999078, China; [2]Institute of Functional Nano & Soft Materials, Jiangsu Key Laboratory for Carbon-Based Functional Materials & Devices, Joint International Research Laboratory of Carbon-Based Functional Materials and Devices, Soochow University, Suzhou 215123, China; [3]Jiangsu Engineering Laboratory of Novel Functional Polymeric Materials, Jiangsu Key Laboratory of Advanced Negative Carbon Technologies, College of Chemistry, Chemical Engineering and Materials Science, Soochow University, Suzhou 215123, China.

†These authors contributed equally to this work.

*Correspondence: XD Wang, E-mail: wangxuedong@suda.edu.cn; LS Liao, E-mail: lsliao@suda.edu.cn

Received: 15 January 2023; Accepted: 24 April 2023; Published online: 18 July 2023

vision, bioimaging, and information-secured displays, are still in challenge[6–10] because of i) the intrinsic fast nonradiative decay of narrow band gap organic materials according to the energy gap law[11,12] and ii) the lack of an effective energy-level system[13]. An effective energy-level system can lead to easier population inversion despite fast nonradiative decay, which can result in low-threshold lasing through stimulated emission[5]. For most organic laser-active materials, a quasi-four-energy level system can be constructed by vibronic levels of the ground state (S_0) and the first excited state (S_1), which cannot be guaranteed when the band gap between S_0 and S_1 becomes sufficiently small[14]. Therefore, constructing an effective energy level system is the key to achieving low-threshold NIR organic lasers.

In recent years, various strategies have been developed to construct four-level systems, such as the introduction of excimers[15], charge transfer[16,17], energy transfer[18,19], cocrystal engineering[20–23], and excited-state intramolecular proton transfer (ESIPT)[24,25]. Therein, in the ESIPT process, a real four-level system can be formed by four electronic energy levels: S_0 and S_1 energy levels of the normal form and S_0 and S_1 energy levels of the tautomer form[26–28]. To date, benefiting from the ESIPT mechanism, a large number of organic gain materials with high gain properties have been successfully developed based on 3-hydroxyflavone[29], 1,5-dihydroxyanthraquinone[30,31], 2-(2'-hydroxyphenyl)benzothiazole[24,32], 10-hydroxybenzo[*h*]quinoline[33]2'-hydroxychalcone[25,34,35], etc. For most of these organic gain materials, the resulting laser emissions are in the visible region. Recently, several approaches were employed to expand the lasing wavelength to the NIR range. For example, by introducing intramolecular charge transfer interactions, a series of donor-acceptor type 2'-hydroxychalcone derivatives have been designed and synthesized by our group and others, which showed deep-red to NIR laser emissions with low thresholds[36–40]. Similarly, Schiff base molecules were also reported as gain materials of organic nonlinear optical lasers with deep-red emission[41]. By further expanding the conjugated system and introducing a cascaded excited-state intramolecular double proton transfer (ESDPT) process, organic lasers with emission wavelengths toward 900 nm can be achieved[42,43]. Nevertheless, earlier studies were mainly focused on individual cases without universal molecular design strategies. Furthermore, the molecular structure and property relationship is unclear for most NIR organic gain materials.

Considering the deficiencies in NIR organic gain materials, a general molecular design strategy of "merging two in one" was developed in this work. By merging two molecules of previously reported 2'-hydroxychalcone derivatives into one new molecule in a centrosymmetric way, a series of NIR organic gain materials were designed and synthesized, which not only dramatically expanded the conjugated systems but also provided molecular structures for the ESDPT process[44]. Compared with the template molecules, all of our newly developed materials exhibited dramatically redshifted photoluminescence (PL) when dissolved in dichloromethane and doped in polystyrene (PS) films. In addition, the ESDPT process can proceed smoothly in these molecules according to the theoretical calculation and experimental results of steady state and transient spectra. Laser performance studies showed that all the materials can achieve ESDPT lasing around 720 nm, which proved the feasibility of the "merging two in one" strategy in the development of NIR laser-active materials. More importantly, our newly designed materials also exhibited high laser stability that can maintain a relatively high laser intensity after 12000 pulses of consecutive excitation. We believe that the described molecular design strategy in this work is transferrable to other ESIPT-active gain materials and will ultimately stimulate the development of NIR organic lasers.

Results and discussion

Molecular design and synthesis

As shown in Fig. 1(a), three D-π-A type 2'-hydroxychalcone derivatives, HPMP, HPPP and HPJP (the IUPAC names for all the compounds can be seen in Supplementary information), with different electron donor groups, were chosen as the template molecules. By merging two identical template molecules into one new molecule in a centrosymmetric way, new molecules can be formed with not only dramatically expanded conjugated systems but also two groups of intramolecular hydrogen bonds, which provides the possibility of the ESDPT process. The syntheses of the model and target molecules are shown in Schemes S1 and S2. HPMP, HPPP and HPJP were synthesized according to a previously reported method[25]. DHN-DMP, DHN-DPP and DHN-DJP (Fig. 1(a)) were synthesized according to our newly designed synthetic route. Taking DHN-DMP as an example, the synthetic route was started from our previously reported

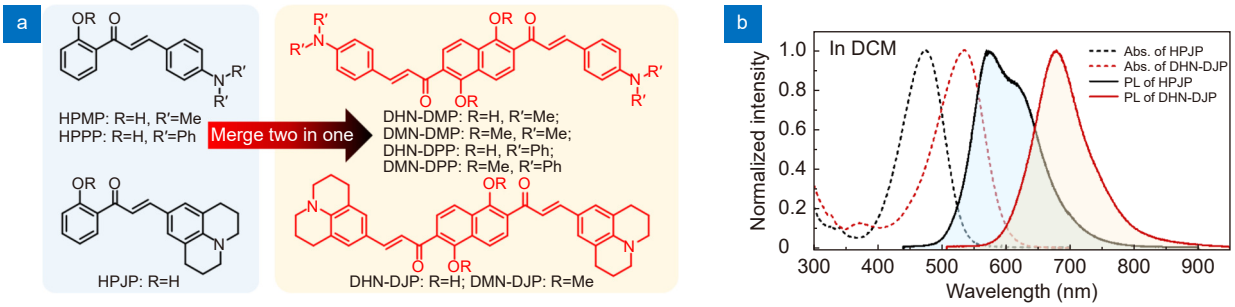

Fig. 1 | (**a**) Chemical structures of the template and target compounds. (**b**) The normalized UV–vis absorption and PL spectra of HPJP and DHN-DJP in DCM solutions.

compound 3, which can be converted into DMN-DMP through a Claisen–Schmidt condensation reaction with compound 2. Subsequently, the target compound DHN-DMP can be successfully synthesized by a demethylation reaction of DMN-DMP. DHN-DPP and DHN-DJP can be obtained using the same method. The chemical structures of all target compounds were characterized by single crystal X-ray diffractions (Figs. S1–S3 and Tables S1–S3). The intermediates DMN-DMP, DMN-DPP and DMN-DJP were also investigated for comparison.

Photophysical properties

The ultraviolet-visible (UV-vis) absorption and steady state photoluminescent (PL) spectra in dichloromethane (DCM, 10^{-5} M) of all materials were measured at room temperature (Fig. S2 and 1(b)). The maximal absorption wavelengths of HPMP and HPPP are approximately 440 nm, and the maximal absorption wavelength of HPJP is 475 nm, indicating stronger electronic coupling between the donor and acceptor of HPJP in the ground state. All newly designed molecules show redshifted absorption peaks, mainly because the expanded conjugated systems can effectively lower the highest occupied molecular orbital-lowest unoccupied molecular orbital (HOMO-LUMO) energy gap[45,46]. Compared with DHN-DMP and DHN-DPP, DHN-DJP also showed stronger electronic coupling between the donor and acceptor in the ground state for a 35-nm redshifted absorption (535 nm for DHN-DJP and 500 nm for DHN-DMP and DHN-DPP). Analogously, the PL spectra of all newly designed molecules exhibit obvious redshifts compared with their template molecules. Next, the UV-vis absorption and PL spectra of the target and template molecules were measured by doping them into polystyrene (PS) at a concentration of 1.0 wt%, which showed similar trends to those in DCM solutions, indicating that redshifted emission can be successfully achieved by the "merge two in one" strategy.

To better understand the effect of our molecular strategy on the photophysical properties, the photoluminescence quantum yields (PLQYs) of these 6 molecules in DCM solutions and in PS films were carefully tested. In general, the PLQYs in PS films are higher than those in DCM solution owing to the effective suppression of molecular vibrations in PS films. The results also showed that the PLQYs of the target compounds were much higher than those of the template compounds in both DCM solutions and PS films, possibly because the stimulated emission cross-sections of the target compounds were dramatically enhanced. DHN-DJP showed the highest PLQYs (3.2% in DCM solution and 7.1% in PS film), which were much higher than those of DHN-DMP and DHN-DPP. This indicates that the julolidine group of DHN-DJP can effectively immobilize the amino group and inhibit molecular vibration[47]. DHN-DPP showed the lowest PLQYs (0.8% in DCM solution and 1.4% in PS film) because of the vibration and rotation of the triphenylamine group. The low PLQYs of our designed materials mainly result from the fast nonradiative decay according to the energy gap law.

ESIPT processes

Subsequently, we studied the ESIPT processes of our target compounds. Every molecule contains two groups of resonance-assisted hydrogen bonds (RAHBs)[31], which provide the structural basis for two ESIPT processes. As shown in Fig. 2(a), tautomer A (TA) can be formed after the first ESIPT process, and tautomer B (TB) can be formed if the second ESIPT can proceed smoothly. To determine the thermodynamic properties of the ESDPT process, density functional theory (DFT) calculations at the TD-DFT/B3LYP/6-31+G(d,p) level were performed with DHN-DMP as an example. As shown in Fig. 2(b), the first ESIPT process can go smoothly because there is

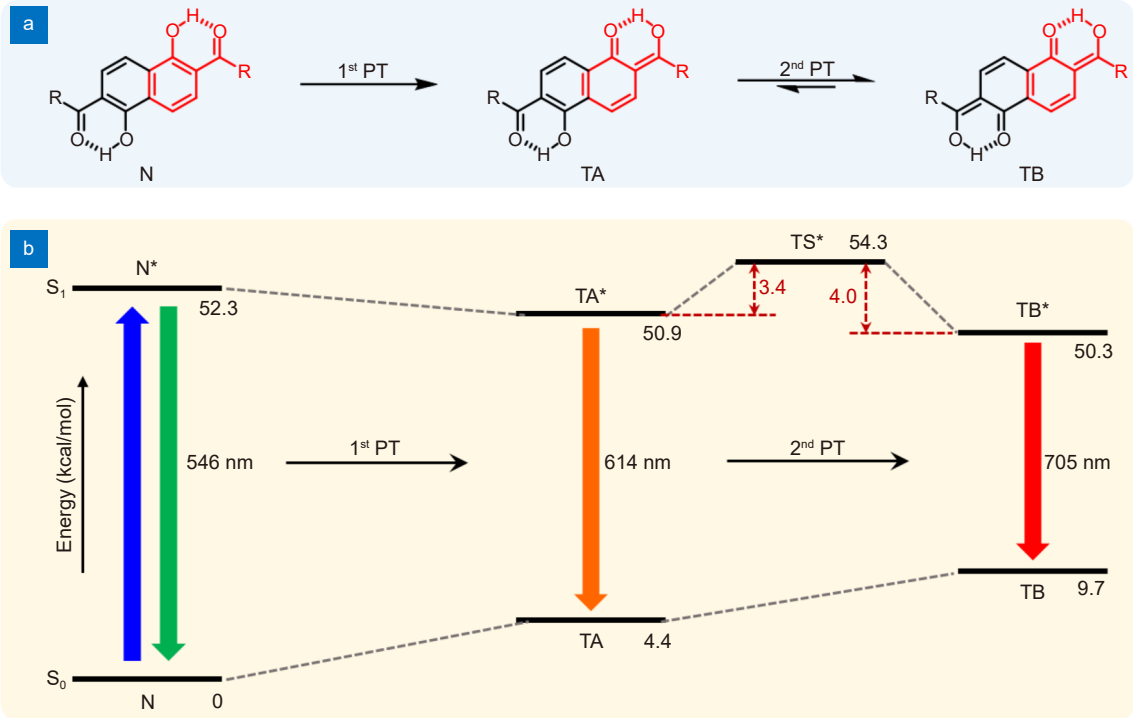

Fig. 2 | (**a**) Diagram of the ESDPT process in DHNs. (**b**) Calculated relative energies (kcal/mol) on S_0 and S_1 of DHN-DMP in vacuum.

no energy barrier and transition state between N* and TA* ("*" means excited state). For the second ESIPT process, a transition state (TS*) can be found between TA* and TB*, and a 3.4 kcal/mol energy barrier has to be crossed. Compared with TA*, the energy level of TB* is slightly lower, which indicates that TB* is relatively more stable than TA*. As the energy level is low enough to get over with the help of thermal activation at room temperature, the proton transfer process from TA* to TB* can occur in thermodynamics. From this point of view, proton transfer from TB* to TA* is also possible in thermodynamics, for which the energy barrier is 4.0 kcal/mol. Therefore, the second ESIPT process may be inversible, and TA* and TB* coexist in the excited state. After radiative transition processes from TA* and TB*, unstable TA and TB can be formed in the ground state. The reverse proton transfer processes can proceed smoothly from TB to TA and from TA to the normal form (N) without any energy barrier.

Next, the UV–vis absorption and PL spectra of DMN-DMP, DMN-DPP and DMN-DJP both in DCM solutions and PS films were tested as comparation, for which no ESIPT process can occur because of the absence of RAHBs. As shown in Figs. S8 and 3, both the absorption and emission peaks of DMNs (DMN-DMP, DMN-DPP and DMN-DJP are collectively called DMNs here) show dramatically hypochromatic shifts compared with those of DHNs (DHN-DMP, DHN-DPP and DHN-DJP are collectively called DHNs here). The PL peaks of DMNs are in accordance with the calculation results of N* emission, indicating that there is no N* emission in the PL spectra of DHNs. In all PL spectra of the DHNs, two peaks can be observed, in accordance with the calculated TA* and TB* emissions, which proved the coexistence of TA* and TB* emissions. The ESDPT process can be further demonstrated by the fluorescent lifetimes of DHNs in PS films at different wavelengths (Fig. 3(b), 3(d) and 3(f)). As shown in Fig. 3(b), both the decay transients at 650 nm and 685 nm involve two decay components ($\tau_1 \approx$ 0.4 ns and $\tau_2 \approx$ 1.0 ns), which may be assigned to the lifetimes of TA* and TB* emissions for the partial coincidence of these two emission peaks. Similar phenomena can be observed for DHN-DPP and DHN-DJP (Fig. 3(d) and 3(f)), indicating the universality of the ESDPT process in our designed DHNs.

To further confirm the ESDPT process, the transient absorption of DHN-DPP in PS film was measured. As shown in Fig. S9, a small peak of the excited-state absorption (ESA) can be observed at 0.2 ps, and the intensity of the peak raised gradually before 0.6 ps. It indicates that a new excited state is formed after 0.2 ps. Interestingly, a new peak emerged after 0.4 ps, which became the major peak gradually. The intensity of the ESA peaks reached a maximum at 0.7 ps and only one broad peak

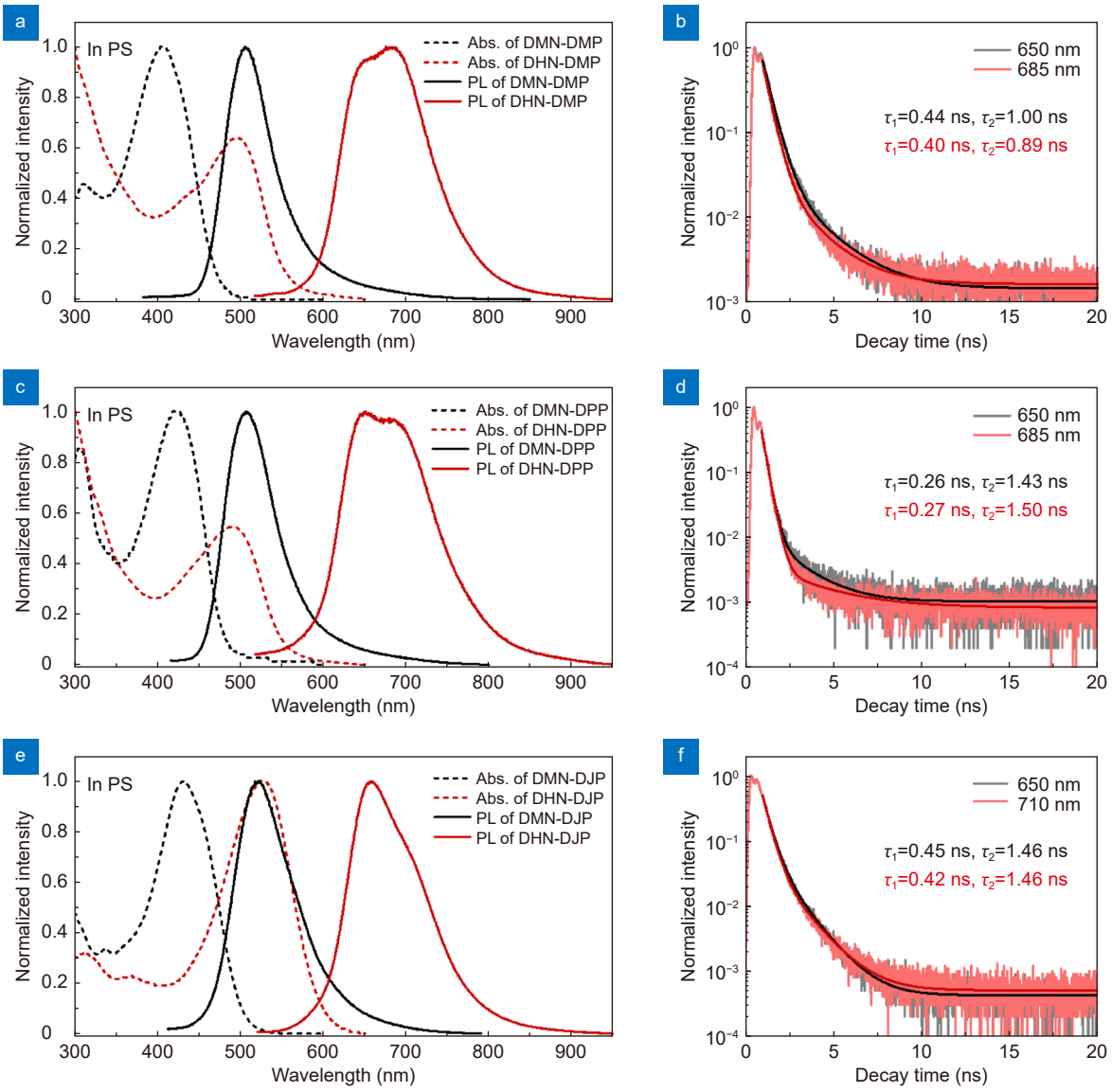

Fig. 3 | (**a**, **c**, **e**) The normalized UV–vis absorption and PL spectra of DMN- and DHN-doped PS films. (**b**, **d**, **f**) The decay plots and fitted curves of DHNs.

can be observed because of the overlap of these two peaks. Afterwards, the intensity of the broad peak decreased gradually without new peak formed. According to the previously reported work, the ESIPT process should be very fast (k_{ept} > 10^{12} s^{-1})[26–28]. Therefore, the first ESA peak can be assigned to TA* state which can be formed in 0.2 ps. The second ESA peak should be assigned to TB* state which can only be formed on the basis of TA* state. Because of the lower relative energy, TB* should be the major excited state when the equilibrium formed between TA* and TB*, which is in accordance with the phenomenon that the second peak became the major peak at 0.7 ps. Overall, the ESDPT process of our designed molecules can be further proved by transient absorption spectrum. It is worth noting that, this kind of ESDPT process is not easy to achieved due to the fact that most of reported molecules containing two groups of intramolecular hydrogen bonds were proved to carry out only one ESIPT process[44,48–50]. Although several molecules have been reported to be able to realize ESDPT or cascaded ESDPT process, our designed molecules are still very important in the mechanism study of ESDPT process[51–53].

From the results of DFT calculations and experimental results, an ESDPT process of target compounds can be supposed, as shown in Fig. S10. First, the target molecules can be excited into N* by excitation light. N* is unstable and can be converted into TA* through the first ESIPT process. TA* can go through the second reversible ESIPT process; as a result, a balance can be formed

between TA* and TB*. Then, TA* and TB* fluoresce through radiative transition, generating TA and TB, respectively. TB can undergo a reverse proton transfer process to form TA, and TA can undergo a second reverse proton transfer process to form N. At this point, the ESDPT process is completed. In this process, light absorption occurs in the N form, and light emission occurs in the TA and TB forms. For TA* emissions, a four-level system can be formed, which is essential for stimulated emissions. For TB* emission, a more effective six-level system can be formed, which was proven to achieve lasing more effectively[42,43]. More importantly, the further energy decay in the second ESIPT process can induce a narrower emission bandgap, resulting in a redshifted emission. Therefore, the introduction of the ESDPT process is a practical strategy in the development of NIR laser materials.

Laser performance

To study the laser performances of our newly developed molecules, DHN-doped PS microspheres were prepared according to a previously reported method[43]. As the UV–vis absorption and PL spectra were not dramatically changed with increasing doping concentration (Fig. S11), 1 wt% was chosen as the doping concentration to maintain their monomolecular properties. As shown in Fig. 4(a), PS microspheres with regular morphology and smooth surfaces can function as whispering gallery-mode (WGM) optical cavities[54,55], and evenly dispersed DHN can be used as gain media so that laser devices can be easily constructed under the pumping of pulsed lasers. Figure S12 shows the bright-field image of a selected single microsphere, and Fig. 4(b) shows the corresponding PL micrograph, showing evenly deep-red emission. The scanning electron microscopy image (inset in Fig. 4(b)) of a single PS microsphere exhibits a perfect circular boundary and ultrasmooth surface. The PL spectra were collected with a homemade micro-photoluminescence system (Fig. S13), which showed a series of sharp resonance peaks (Fig. 4(c)). The space between the individual resonance peaks ($\Delta\lambda$) increases with increasing emission wavelength and decreasing dimeter (D) of the

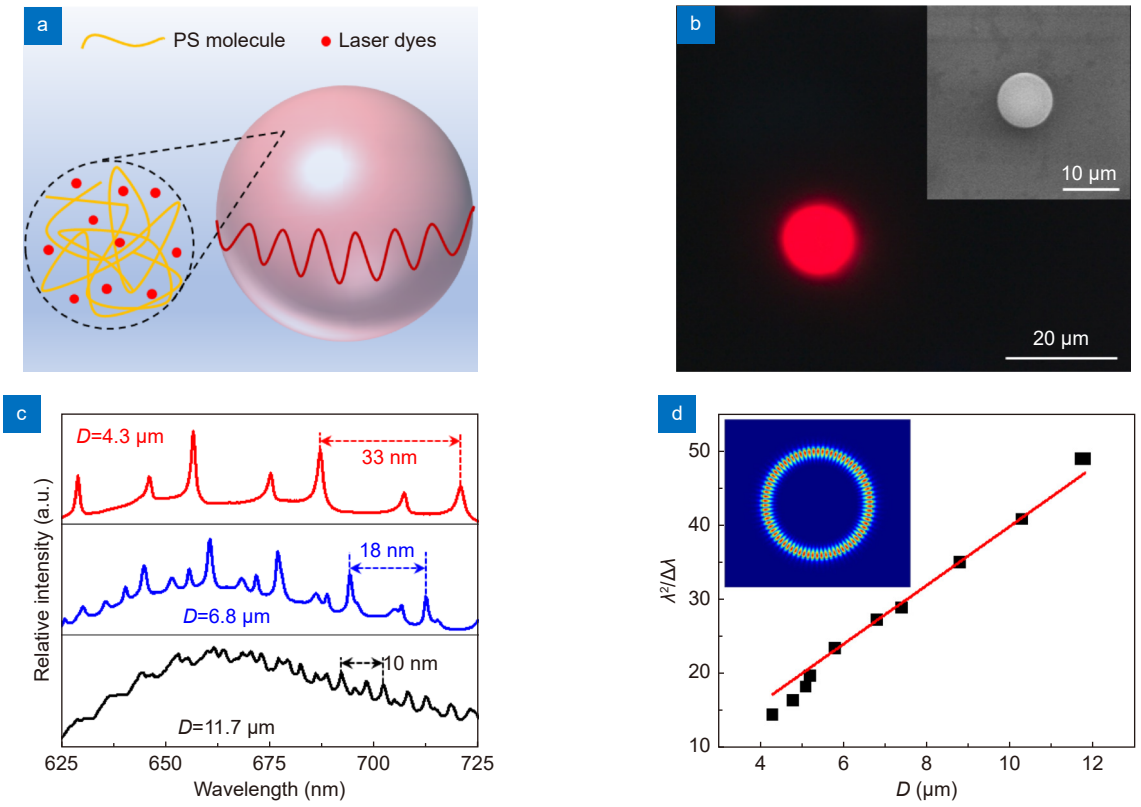

Fig. 4 | (**a**) Schematic diagram of a single DHN-doped microsphere. (**b**) PL micrograph of a single DHN-doped microsphere. Inset: scanning electron microscopy image of a single DHN-doped microsphere. (**c**) Partial magnifications of PL spectra of DHN-doped microspheres with different sizes. (**d**) The related curve of $\lambda^2/\Delta\lambda$ (λ: emission wavelength; $\Delta\lambda$: the space between the individual resonance peaks) at 700 nm versus D (D: diameter of selected microsphere). Inset: the simulated electric energy density in the cross-section of a microsphere with dimeter D = 10 μm. Red corresponds to the highest field density and blue is the lowest field density.

individual microsphere. Figure 4(d) shows a good linear relationship between $\lambda^2/\Delta\lambda$ at the 700 nm position versus D of the PS microsphere, conforming to the typical characteristics of a WGM resonator[56].

The laser performances of DHNs were next studied with a 532 nm nanosecond pulsed laser as the pumping source. With the increase of the pumping density, a set of laser peaks with a center wavelength around 720 nm gradually emerged (Fig. 5(a, d, g)). From the above analyses, the laser emission at 720 nm should be assigned to TB* emission, which, in turn, proved the ESDPT process in DHNs. Figure 4(b, e, h) show the relationship between the PL intensity and pumping density of DHN-DMP-, DHN-DPP- and DHN-DJP-doped microspheres, from which the lasing thresholds were calculated as 26.6, 18.4 and 16.7 μJ/cm², respectively. The quality factors (Q) of these three microsphere-lasers were calculated as 1964, 1075 and 909 respectively according to their full width at half maximum intensity (FWHMs) and peak wavelengths ($Q = \lambda/\lambda_{FWHM}$)[37]. The difference of the Q factors may result from the difference of the qualities of the microspheres which were selected in random. DHN-DJP-doped microspheres showed the lowest lasing threshold despite the lowest Q factor, agreeing with the highest PLQY of DHN-DJP among these three molecules. DHN-DMP-doped microspheres showed the highest lasing threshold and the highest Q factor, possibly because of the localized aggregation-caused quenching induced by the strong intermolecular interaction between two adjacent DHN-DMP molecules[45]. For DHN-DPP, the large steric hindrance of the triphenylamine group can prevent localized aggregation. As a result, DHN-DPP-doped PS microspheres exhibit a relatively low lasing threshold. For comparison, we also tested the laser performance of DMN-DJP-doped PS microspheres. A 355-nm pulsed laser was used as the

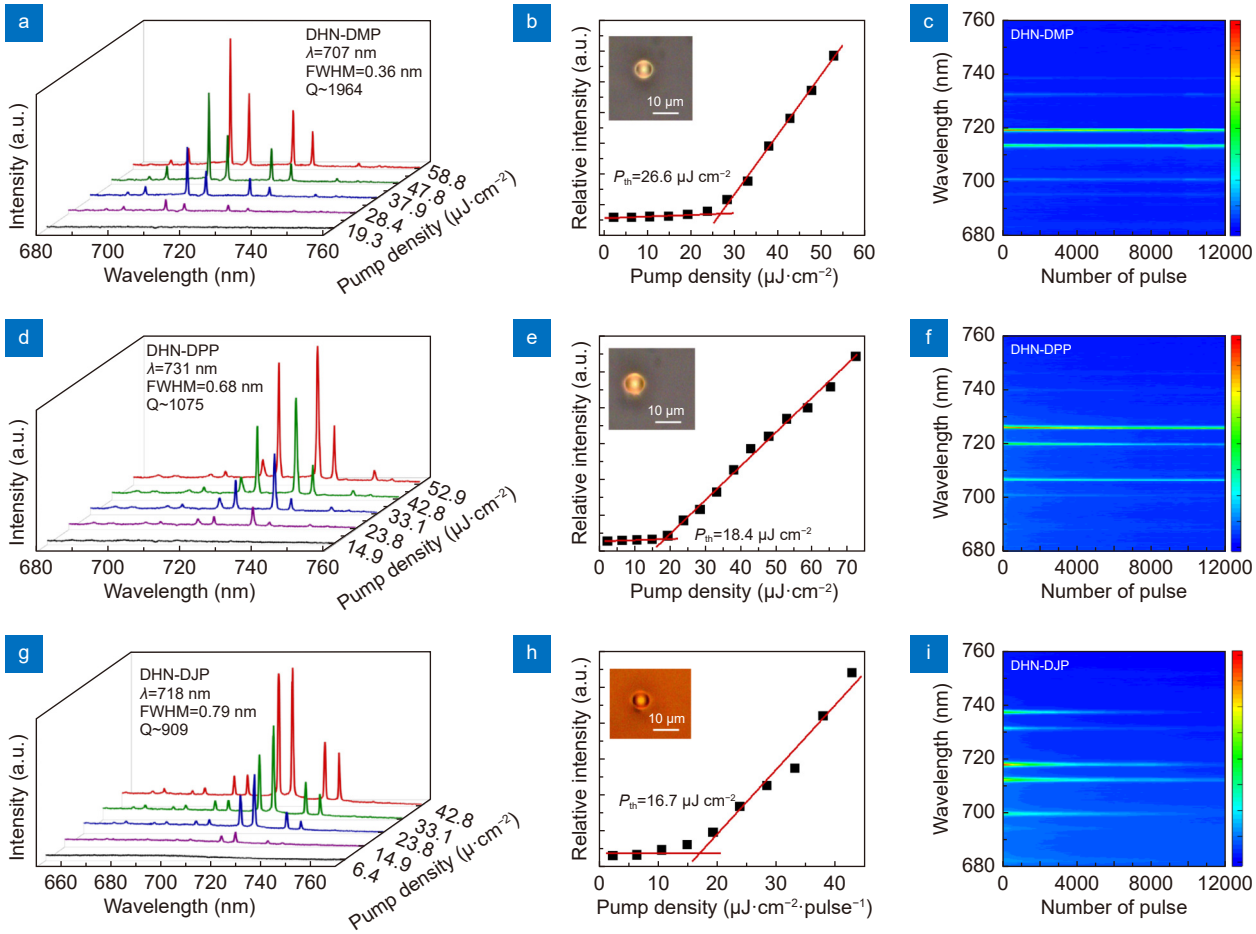

Fig. 5 | PL spectra of (**a**) DHN-DMP-, (**d**) DHN-DPP- and (**g**) DHN-DJP-doped PS microspheres under different pump densities. (b) Plots of lasing intensity as a function of pump density of a (**b**) DHN-DMP-, (**e**) DHN-DPP- and (**h**) DHN-DJP-doped PS microsphere. Insets: brightfield micrographs of the PS microspheres used in laser measurements. (**c**) 2D mappings of lasing intensity versus the number of pulses of a (c) DHN-DMP-, (**f**) DHN-DPP- and (**i**) DHN-DJP-doped PS microsphere, pumping density: 47.8 μJ/cm².

pumping source according to the absorption spectrum. In contrast, no laser emission or spectral narrowing can be observed when we gradually increase the pumping density (Fig. S14). This indicates that laser emission cannot be easily achieved without an effective energy level system.

To investigate the laser stability of the PS microspheres doped with our new gain materials, the laser emissions were measured for 12000 pulses consecutively at a pumping density of 47.8 μJ/cm^2. As shown in Fig. 5(c) and 5(f), for the PS microspheres doped with DHN-DMP and DHN-DPP, the laser intensities were still kept at a high level after 12000 excitations. From Fig. S15, we can find that DHN-DPP-doped PS microspheres showed the best laser stability. For DHN-DJP-doped microspheres, the laser emission is much less stable due to the obviously reduced laser intensity (Fig. 5(i) and S15(c)). In general, the degradation of gain materials is regarded as the main factor in laser deactivation[57]. From the view of the chemical structures of our new molecules, the julolidine group in DHN-DJP is more electron-rich and, as a result, more easily oxidized by oxygen from air. For DHP-DPP, the phenyl groups in the triphenylamine group can effectively reduce the electron density of the nitrogen atom by the conjugation effect, which stabilizes the molecular structure in air. Overall, our newly developed NIR organic lasers are much more stable than those in previously reported work.

Conclusions

In summary, we have developed an effective molecular design strategy for NIR organic gain materials by merging two in one, by which three new molecules, DHN-DMP, DHN-DPP and DHN-DJP, were designed and synthesized based on previously reported 2'-hydroxychalcone derivatives. All these new materials showed dramatically redshifted emission compared with their templated molecules. DFT calculations and spectral studies indicated that the redshifts are attributed to not only the expansion of conjugated systems but also the ESDPT process. We demonstrated that the first ESIPT process can proceed without any energy barrier; however, the second ESIPT process is inversible and, as a result, reaches a balance between TA* and TB*. Laser performance studies showed that all the materials can achieve NIR lasing from the TB* state, indicating the advantage of the six-level system in achieving stimulated emission. Furthermore, the structure and property relationships of our development gain materials are also systematically investigated, demonstrating that both intramolecular and intermolecular interactions can affect the laser performance. It is worth mentioning that our developed organic lasers showed high stability; in particular, the DHN-DPP-based laser can maintain high laser intensity after 12000 pulses. This study not only provided a practical method for the development of new organic laser-active materials but also demonstrated an ESDPT mechanism for NIR lasing, which will facilitate the development and practical applications of NIR organic lasers.

References

1. Jiang Y, Liu YY, Liu X, Lin H, Gao K et al. Organic solid-state lasers: a materials view and future development. *Chem Soc Rev* **49**, 5885–5944 (2020).
2. Kuehne AJC, Gather MC. Organic lasers: recent developments on materials, device geometries, and fabrication techniques. *Chem Rev* **116**, 12823–12864 (2016).
3. Yan CC, Wang XD, Liao LS. Thermally activated delayed fluorescent gain materials: harvesting triplet excitons for lasing. *Adv Sci* **9**, 2200525 (2022).
4. Wei GQ, Wang XD, Liao LS. Recent advances in 1D organic solid-state lasers. *Adv Funct Mater* **29**, 1902981 (2019).
5. Wu JJ, Wang XD, Liao LS. Advances in energy-level systems of organic lasers. *Laser Photonics Rev* **16**, 2200366 (2022).
6. Wang Y, Yu JY, Mao YF, Chen J, Wang S et al. Stable, high-performance sodium-based plasmonic devices in the near infrared. *Nature* **581**, 401–405 (2020).
7. Ma RM, Oulton RF. Applications of nanolasers. *Nat Nanotechnol* **14**, 12–22 (2019).
8. Hong GS, Antaris AL, Dai HJ. Near-infrared fluorophores for biomedical imaging. *Nat Biomed Eng* **1**, 0010 (2017).
9. Hill MT, Gather MC. Advances in small lasers. *Nat Photonics* **8**, 908–918 (2014).
10. Yan RX, Gargas D, Yang PD. Nanowire photonics. *Nat Photonics* **3**, 569–576 (2009).
11. Wei YC, Wang SF, Hu Y, Liao LS, Chen DG et al. Overcoming the energy gap law in near-infrared OLEDs by exciton–vibration decoupling. *Nat Photonics* **14**, 570–577 (2020).
12. Caspar JV, Kober EM, Sullivan BP, Meyer TJ. Application of the energy gap law to the decay of charge-transfer excited states. *J Am Chem Soc* **104**, 630–632 (1982).
13. Wu JJ, Wang XD, Liao LS. Near-infrared solid-state lasers based on small organic molecules. *ACS Photonics* **6**, 2590–2599 (2019).
14. Gierschner J, Varghese S, Park SY. Organic single crystal lasers: a materials view. *Adv Opt Mater* **4**, 348–364 (2016).
15. Wei C, Gao MM, Hu FQ, Yao JN, Zhao YS. Excimer emission in self-assembled organic spherical microstructures: an effective approach to wavelength switchable microlasers. *Adv Opt Mater* **4**, 1009–1014 (2016).
16. Dong HY, Wei YH, Zhang W, Wei C, Zhang CH et al. Broadband tunable microlasers based on controlled intramolecular charge-transfer process in organic supramolecular microcrystals. *J Am Chem Soc* **138**, 1118–1121 (2016).

17. Wei YH, Dong HY, Wei C, Zhang W, Yan YL et al. Wavelength-tunable microlasers based on the encapsulation of organic dye in metal–organic frameworks. *Adv Mater* **28**, 7424–7429 (2016).
18. Wang K, Gao ZH, Zhang W, Yan YL, Song HW et al. Exciton funneling in light-harvesting organic semiconductor microcrystals for wavelength-tunable lasers. *Sci Adv* **5**, eaaw2953 (2019).
19. Okada D, Azzini S, Nishioka H, Ichimura A, Tsuji H et al. π-Electronic co-crystal microcavities with selective vibronic-mode light amplification: toward förster resonance energy transfer lasing. *Nano Lett* **18**, 4396–4402 (2018).
20. Lin HT, Ma YX, Chen S, Wang XD. Hierarchical integration of organic core/shell microwires for advanced photonics. *Angew Chem Int Ed* **62**, e202214214 (2023).
21. Lv Q, Wang XD, Yu Y, Zhuo MP, Zheng M et al. Lattice-mismatch-free growth of organic heterostructure nanowires from cocrystals to alloys. *Nat Commun* **13**, 3099 (2022).
22. Ma YX, Chen S, Lin HT, Zhuo SP, Wang XD. Organic low-dimensional crystals undergoing twinning deformation. *Sci Bull* **67**, 1632–1635 (2022).
23. Su Y, Yao ZF, Wu B, Zhao YD, Han JY et al. Organic polymorph-based alloys for continuous regulation of emission colors. *Matter* **5**, 1520–1531 (2022).
24. Zhang W, Yan YL, Gu JM, Yao JN, Zhao YS. Low-threshold wavelength-switchable organic nanowire lasers based on excited-state intramolecular proton transfer. *Angew Chem Int Ed* **54**, 7125–7129 (2015).
25. Cheng X, Wang K, Huang S, Zhang HY, Zhang HY et al. Organic crystals with near-infrared amplified spontaneous emissions based on 2'-hydroxychalcone derivatives: subtle structure modification but great property change. *Angew Chem Int Ed* **54**, 8369–8373 (2015).
26. Yan CC, Wang XD, Liao LS. Organic lasers harnessing excited state intramolecular proton transfer process. *ACS Photonics* **7**, 1355–1366 (2020).
27. Padalkar VS, Seki S. Excited-state intramolecular proton-transfer (ESIPT)-inspired solid state emitters. *Chem Soc Rev* **45**, 169–202 (2016).
28. Kwon JE, Park SY. Advanced organic optoelectronic materials: harnessing excited-state intramolecular proton transfer (ESIPT) process. *Adv Mater* **23**, 3615–3642 (2011).
29. Chou P, McMorrow D, Aartsma TJ, Kasha M. The proton-transfer laser. Gain spectrum and amplification of spontaneous emission of 3-hydroxyflavone. *J Phys Chem* **88**, 4596–4599 (1984).
30. Wei GQ, Yu Y, Zhuo MP, Wang XD, Liao LS. Organic single-crystalline whispering-gallery mode microlasers with efficient optical gain activated *via* excited state intramolecular proton transfer luminogens. *J Mater Chem C* **8**, 11916–11921 (2020).
31. Yang WY, Lai RC, Wu JJ, Yu YJ, Yan CC et al. Deepening insights into near-infrared excited-state intramolecular proton transfer lasing: the charm of resonance-assisted hydrogen bonds. *Adv Funct Mater* **32**, 2204129 (2022).
32. Mai VTN, Shukla A, Mamada M, Maedera S, Shaw PE et al. Low amplified spontaneous emission threshold and efficient electroluminescence from a carbazole derivatized excited-state intramolecular proton transfer dye. *ACS Photonics* **5**, 4447–4455 (2018).
33. Chen KY, Hsieh CC, Cheng YM, Lai CH, Chou PT. Extensive spectral tuning of the proton transfer emission from 550 to 675 nm via a rational derivatization of 10-hydroxybenzo[h]quinoline. *Chem Commun* **42**, 4395–4397 (2006).
34. Wang XD, Liao Q, Lu XM, Li H, Xu ZZ et al. Shape-engineering of self-assembled organic single microcrystal as optical microresonator for laser applications. *Sci Rep* **4**, 7011 (2014).
35. Cheng X, Zhang YF, Han SH, Li F, Zhang HY et al. Multicolor amplified spontaneous emissions based on organic polymorphs that undergo excited-state intramolecular proton transfer. *Chem Eur J* **22**, 4899–4903 (2016).
36. Che ZL, Yan CC, Wang XD, Liao LS. Organic near-infrared luminescent materials based on excited state intramolecular proton transfer process. *Chin J Chem* **40**, 2468–2481 (2022).
37. Wang XD, Liao Q, Li H, Bai SM, Wu YS et al. Near-infrared lasing from small-molecule organic hemispheres. *J Am Chem Soc* **137**, 9289–9295 (2015).
38. Wang XD, Li ZZ, Zhuo MP, Wu YS, Chen S et al. Tunable near-infrared organic nanowire nanolasers. *Adv Funct Mater* **27**, 1703470 (2017).
39. Wang XD, Li ZZ, Li SF, Li H, Chen JW et al. Near-infrared organic single-crystal lasers with polymorphism-dependent excited state intramolecular proton transfer. *Adv Opt Mater* **5**, 1700027 (2017).
40. Wu JJ, Gao HF, Lai RC, Zhuo MP, Feng JG et al. Near-infrared organic single-crystal nanolaser arrays activated by excited-state intramolecular proton transfer. *Matter* **2**, 1233–1243 (2020).
41. Venkatakrishnarao D, Narayana YSLV, Mohaiddon MA, Mamonov EA, Mitetelo N et al. Two-photon luminescence and second-harmonic generation in organic nonlinear surface comprised of self-assembled frustum shaped organic microlasers. *Adv Mater* **29**, 1605260 (2017).
42. Wu JJ, Zhuo MP, Lai RC, Zou SN, Yan CC et al. Cascaded excited-state intramolecular proton transfer towards near-infrared organic lasers beyond 850 nm. *Angew Chem Int Ed* **60**, 9114–9119 (2021).
43. Yan CC, Liu YP, Yang WY, Wu JJ, Wang XD et al. Excited-state intramolecular proton transfer parent core engineering for six-level system lasing toward 900 nm. *Angew Chem Int Ed* **61**, e202210422 (2022).
44. Yang WY, Yan CC, Wang XD, Liao LS. Recent progress on the excited-state multiple proton transfer process in organic molecules. *Sci China Chem* **65**, 1843–1853 (2022).
45. Aoki R, Komatsu R, Goushi K, Mamada M, Ko SY et al. Realizing near-infrared laser dyes through a shift in excited-state absorption. *Adv Opt Mater* **9**, 2001947 (2021).
46. Yan CC, Wu JJ, Yang WY, Chen S, Lv Q et al. Precise synthesis of multilevel branched organic microwires for optical signal processing in the near infrared region. *Sci China Mater* **65**, 1020–1027 (2022).
47. Mao WY, Tang J, Dai LQ, He XY, Li J et al. A general strategy to design highly fluorogenic far-red and near-infrared tetrazine bioorthogonal probes. *Angew Chem Int Ed* **60**, 2393–2397 (2021).
48. Lim SJ, Seo J, Park SY. Photochromic switching of excited-state intramolecular proton-transfer (ESIPT) fluorescence: a unique route to high-contrast memory switching and nondestructive readout. *J Am Chem Soc* **128**, 14542–14547 (2006).
49. Zhang ZY, Chen YA, Hung WY, Tang WF, Hsu YH et al. Control of the reversibility of excited-state intramolecular proton transfer (ESIPT) reaction: host-polarity tuning white organic light emitting diode on a new thiazolo[5, 4-*d*]thiazole ESIPT system.

Chem Mater **28**, 8815–8824 (2016).

50. Frizon TEA, Salla CAM, Grillo F, Rodembusch FS, Câmara VS et al. ESIPT-based benzazole-pyromellitic diimide derivatives. A thermal, electrochemical, and photochemical investigation. *Spectrochim Acta A Mol Biomol Spectrosc* **288**, 122050 (2023).
51. Peng CY, Shen JY, Chen YT, Wu PJ, Hung WY et al. Optically triggered stepwise double-proton transfer in an intramolecular proton relay: a case study of 1, 8-dihydroxy-2-naphthaldehyde. *J Am Chem Soc* **137**, 14349–14357 (2015).
52. Vérité PM, Guido CA, Jacquemin D. First-principles investigation of the double ESIPT process in a thiophene-based dye. *Phys Chem Chem Phys* **21**, 2307–2317 (2019).
53. Wróblewski T, Ushakou D. Stepwise excited-state double proton transfer and fluorescence decay analysis. *J Fluoresc* **33**, 103–111 (2023).
54. Wei GQ, Wang XD, Liao LS. Recent advances in organic whispering-gallery mode lasers. *Laser Photonics Rev* **14**, 2000257 (2020).
55. Venkatakrishnarao D, Mamonov EA, Murzina TV, Chandrasekar R. Advanced organic and polymer whispering-gallery-mode microresonators for enhanced nonlinear optical light. *Adv Optical Mater* **6**, 1800343 (2018).
56. Wang XD, Liao Q, Kong QH, Zhang Y, Xu ZZ et al. Whispering-gallery-mode microlaser based on self-assembled organic single-crystalline hexagonal microdisks. *Angew Chem Int Ed* **53**, 5863–5867 (2014).
57. Matsushima T, Yoshida S, Inada K, Esaki Y, Fukunaga T et al. Degradation mechanism and stability improvement strategy for an organic laser gain material 4, 4'-Bis[(*N*-carbazole)styryl]biphenyl (BSBCz). *Adv Funct Mater* **29**, 1807148 (2019).

Acknowledgements

We are grateful for financial supports from the National Natural Science Foundation of China (Nos. 52173177, 21971185, 22105139), Fundação Universidade de Ciência e Tecnologia de Macau (No. 0006/2021/AKP), the Natural Science Foundation of Jiangsu Province (No. BK20221362), and the Science and Technology Support Program of Jiangsu Province (No. TJ-2022-002). This project is also funded by Suzhou Key Laboratory of Functional Nano & Soft Materials, Collaborative Innovation Center of Suzhou Nano Science & Technology, the 111 Project, Joint International Research Laboratory of Carbon-Based Functional Materials and Devices, and Soochow University Tang Scholar.

Author contributions

C. C. Yan, X. D. Wang and L. S. Liao proposed the original idea. X. D. Wang and L. S. Liao supervised the project. C. C. Yan, Z. L. Che and W. Y. Yang fabricated the samples and performed the measurements. C. C. Yan, Z. L. Che, X. D. Wang, and L. S. Liao discussed the interpretation of results and wrote the manuscript. All authors discussed the results and commented on the manuscript.

Competing interests

The authors declare no competing financial interests.

Supplementary information

Supplementary information for this paper is available at https://doi.org/10.29026/oea.2023.230007